PAPER

Stress relaxation in the transition from shear thinning to shear jamming in shear thickening fluid

View the article online for updates and enhancements.

Stress relaxation in the transition from shear thinning to shear jamming in shear thickening fluid

Saisai Cao[1], Qianyun He[1], Haoming Pang[1], Kaihui Chen[1], Wanquan Jiang[2] and Xinglong Gong[1]

[1] CAS Key Laboratory of Mechanical Behavior and Design of Materials, Department of Modern Mechanics, University of Science and Technology of China (USTC), Hefei, 230027, People's Republic of China
[2] Department of Chemistry, USTC, Hefei, 230026, People's Republic of China

E-mail: gongxl@ustc.edu.cn

CrossMark

Abstract

The rheological measurement was adopted to study the relationship between the stress relaxation phenomenon and the internal structure of shear thickening fluid (STF). Based on particle chain network, the viscoelastic model successfully predicted the stress relaxation and agreed well with experimental results. By investigating the stress relaxation behavior, it was found the transition from continuous shear thickening to discontinuous shear thickening could occur not only by increasing the volume fraction ϕ but also by increasing the shear rate $\dot{\gamma}$ and shear time t_s. The phase diagram in the $\phi-\dot{\gamma}$ plane revealed the structure transition of STF under shear.

Keywords: nanoparticle, shear thickening fluid, stress relaxation, viscoelastic model, phase diagram

(Some figures may appear in colour only in the online journal)

1. Introduction

Shear thickening fluid (STF) is a kind of dense suspension whose viscosity η dramatically increases as the shear rate $\dot{\gamma}$ exceeds a threshold [1–5]. Suspensions are usually divided into Brownian ($d < 1000$ nm) and non-Brownian ($d > 1000$ nm) suspensions [6–8] based on the diameter of particles. Continuous shear thickening (CST) is used to describe the mild increase in η and it is often observed in suspensions with low particle volume fraction ϕ. In CST suspensions, the hydrodynamic force is dominant, particles aggregate to form locally high concentrations of particle clusters [9], which results in mild increases in viscosity. With the increase of ϕ, the particles are easily to contact with each other to form a force-chain network [10–12], accompanied by an increase in normal force F_N [5, 8, 13], a sharp rise in η and even an S-shaped flow curve [14–16]. In this case, the suspensions change from CST to discontinuous shear thickening (DST) [17–19]. Recent investigations suggest that DST

corresponds to a fragile state instead of a jammed state [20] and the STF exhibits an intermittent flow behavior. Shear jamming (SJ) is proposed to describe a solid-like [21], fully jammed state in dense suspensions under shear [17, 22, 23].

STF can recover to the initial state after removing shear. Due to this reversible behavior, it is widely applied in damping and body armor [24–27], in which the recovery time should be noticed. Therefore, it is necessary to study the time dependence of STF. The time response of STF at constant $\dot{\gamma}$ showed that the change of η was related to its internal structure [28, 29]. Just like thixotropy [30] and creep behavior [31], stress relaxation, which is defined as the decay of shear stress at a constant shear strain, is also used to characterize the time dependence of STF [2, 32–34]. During the past decade, the analysis of stress relaxation behavior of STF was merely a description of the experimental results. Recently, researchers began to take this phenomenon seriously. Hu adopted the double exponential function to fit the stress relaxation curve and got a good fitting result [33]. Brown tested the relaxation
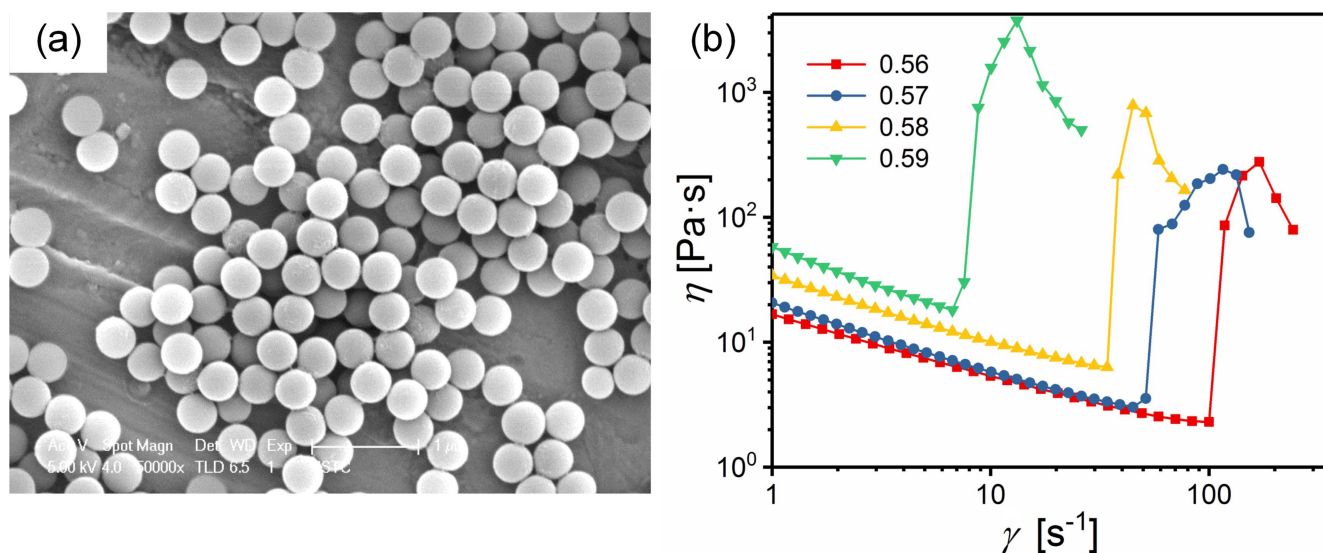
Figure 1. (a) SEM image of PSt-EA nanoparticles. (b) Typical rheological behavior of the STF with different volume fraction.

time of STF using the stress-control and rate-control methods, and found that relaxation behavior of STF was related to volume fraction [34].

Although the existing fitting function can keep relatively high consistency with the experimental results, no phenomenological or theoretical model was proposed to explain the fitting function, which makes it lack of physical meaning. In this paper, the STFs contained polystyrene-ethylacrylate (PSt-EA) nanoparticles were prepared and the stress relaxation behavior of STF was studied through a rheological method. A viscoelastic model and a theoretical model were proposed to explain this behavior. The relationship between relaxation behavior and internal structure of STF in different states was further studied. Finally, the results of stress relaxation with different volume fraction were summarized in a phase diagram to depict the structure evolution of STF under shear.

2. Materials and methods

2.1. Preparation and characterization of PSt-EA nanoparticles

The PSt-EA nanoparticles were prepared by soap free emulsion polymerization. All polymerizations were carried out in a 500 ml three-necked flask fixed with a mechanical stirrer, a reflux condenser and a nitrogen inlet. Styrene (St), ethylacrylate (EA) and acrylate (AA) were firstly mixed using a mechanical stirrer for 30 min in distilled water. Then, the initiator, KPS, which was handled using the recrystallization method, was added to the mixture and mixed for 10 min at room temperature. After that, the flask was heated to 75 °C in a water bath for 6 h. All runs were conducted under nitrogen atmosphere. The emulsion obtained was centrifuged and then the sediment was redispersed in distilled water to be cleaned for 30 min using an ultrasonic cleaner. This procedure was iterated three times. Finally, the PSt-EA nanoparticles obtained were dried in a vacuum oven at 40 °C.

The microstructure of the PSt-EA nanoparticles was investigated by scanning electron microscopy (SEM, Sirion 200). The SEM image of PSt-EA nanoparticles is given in figure 1(a). The microscopy of PSt-EA nanoparticles indicates that the nanoparticles are monodisperse. In addition, this type of nanoparticle is regularly arranged and no terrible aggregations are found. The average particle size of PSt-EA is estimated to be around 340 nm.

2.2. Preparation of STFs and rheological measurement

The STFs were obtained by dispersing the PSt-EA nanoparticles into ethylene glycol (EG). The density of the particles and EG is approximately matched [35]. The suspension was mixed in a ball mill grinding up to about 24 h in order to obtain a uniform distribution. In this research, different concentrations of STFs (0.56, 0.57, 0.58 and 0.59) were prepared by varying the amount of PSt-EA in EG.

The experimental measurements were conducted by a stress and strain controlled rheometer (Anton-Paar MCR 301) with cone-plate geometry (25 mm in diameter and 2 in cone angle). All the experiments were conducted with a gap size of 0.05 mm at a room temperature of 25 °C. A pre-shear was used to provide consistent flow. The steady shear test was first conducted and then the relaxation behavior of STF was investigated.

3. Results and discussion

3.1. Steady shear results of STF

The volume fraction of STF has a significant influence on the shear thickening effect. Figure 1(b) presents the typical viscosity curves of STF with different volume fraction. As the volume fraction increases from 0.56, 0.57, 0.58 to 0.59, the critical shear rate decreases from 100, 45, 34 to 7 s^{-1} and the maximum viscosity increases from 278, 242, 787 to
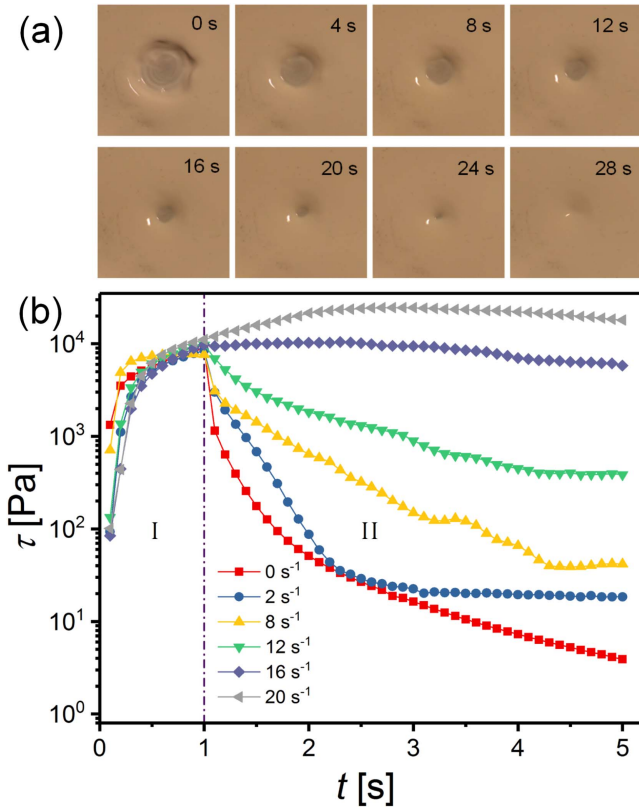
Figure 2. (a) The recovery process of the hole in the STF surface after the treatment of airflow. (b) The shear stress of STF at varies shear rates after a pre-shear stage at $\dot{\gamma} = 20 \, \text{s}^{-1}$.

3765 Pa s, respectively. The shear thickening effect of the suspensions is strengthened with the increasing volume fraction.

3.2. Stress decay under different shear rates

A demonstration experiment was first conducted. The holes in the STF surface were created by two different methods: driven by airflow and impacted with a hammer. Obviously, the strain rate of hammer impact is much larger than the airflow. As shown in figures 2(a), the hole formed by the airflow disappears in tens of seconds, while the other can last a few days. It can be inferred qualitatively that the recovery time of STF is prolonged with the increase of strain rate.

The change of stress cannot be observed while the shape of the hole remains the same in the demonstration experiment. To investigate the time dependence of STF, the rheological measurement was carried out. The STF ($\phi = 0.59$) was first sheared at $20 \, \text{s}^{-1}$ for 1 s (stage I), then $\dot{\gamma}$ was adjusted to 0, 2, 8, 12, 16, $20 \, \text{s}^{-1}$ (stage II). The result is presented in figure 2(b). As shown in figure 1(b), the critical shear rate $\dot{\gamma}_c$ is about $10 \, \text{s}^{-1}$. When $\dot{\gamma} < \dot{\gamma}_c$, the STF shows shear thinning. When $\dot{\gamma} > \dot{\gamma}_c$, the viscosity increases dramatically and the STF performs shear thickening. So the shear stress increases with time at a fixed $\dot{\gamma}$ in stage I. In stage II, shear stress can decrease to a low constant value as $\dot{\gamma}$ is below the critical shear rate $\dot{\gamma}_c$. The decay rate of shear stress generally slows down with the increase of $\dot{\gamma}$. In the ST section, shear stress

decays slowly and can even maintain at very high values, e.g., shear stress can maintain at 10^4 Pa as $\dot{\gamma}$ above $16 \, \text{s}^{-1}$.

3.3. Analytical model

The decay of shear stress at a constant shear strain is defined as stress relaxation. In figure 2(b), the curve at $\dot{\gamma} = 0$ represents the typical stress relaxation of STF. The appearance of ST is accompanied by the formation of 'force-chain' network. So the relaxation stress is related to the evolution of force-chain network. Figure 3(a) presents a schematic diagram of the internal force-chain structure [36] during ST. The particle chains are usually only able to withstand compression and cannot afford to stretch. However, in the model of figure 3(a), the force-chain is a simplification of the system, including particle–particle interaction and liquid–particle interaction. Similar to the macromolecule polymer system [37] in figure 3(b), the interior of the STF can be decomposed into a compressive force in the main chain direction and a tensile force in the sub-chain direction when subjected to shear. The analysis of normal force is complicated and many related investigations have been published [37, 38]. Therefore, it is not described in detail here. The qualitative conclusion is that the normal force of the system is positive when the force along the direction of compression dominates. On the other hand, when the force in the direction of extension dominates, the normal force is negative.

The particles form force-chain structure along the direction of compression at $\dot{\gamma}$. It can be approximated that the particles are in dynamic equilibrium. When $\dot{\gamma} = 0$, the STF continues to decelerate in the previous shear direction. Particle in the middle of the chain can be thought to decelerate with Stokes force. So the equation of motion is:

$$m\ddot{x}_c = -6\pi\eta a\dot{x}_c, \tag{1}$$

where m is the weight of particle, x_c is the displacement of the particle in the middle of the chain, η is the viscosity of solvent, a is the equivalent radius of particle. The force of the particle at the top of chain is shown in figure 3(c). The particle is driven by the elastic force along the chain N_1, the elastic force along other force-bearing particles N_2, the elastic force of the upper plate N_3, Stokes force f_s and frictional force f_f. The equation of motion can be written as:

$$m\ddot{x} = -N_1\sin\theta + N_2\sin\varphi - \mu N_3 - 6\pi\eta a\dot{x}, \tag{2}$$

where θ and φ are the angles between N_1, N_2 and the vertical direction, respectively. The expressions for N_1, N_2 and N_3 are as follows:

$$N_1 = k_1(l_{01} - l), \tag{3}$$

$$N_2 = k_2\left(\frac{l}{2}\Delta\theta - l_{02}\right), \tag{4}$$

$$N_3 = N_1\cos\theta + N_2\cos\varphi, \tag{5}$$

where k_1, k_2 and l_{01}, l_{02} are the stiffness and original length of force-chain structure and force-bearing particles, respectively. l is the length of force-chain structure. Compared with the central particle in force-chain, the top particle is additionally
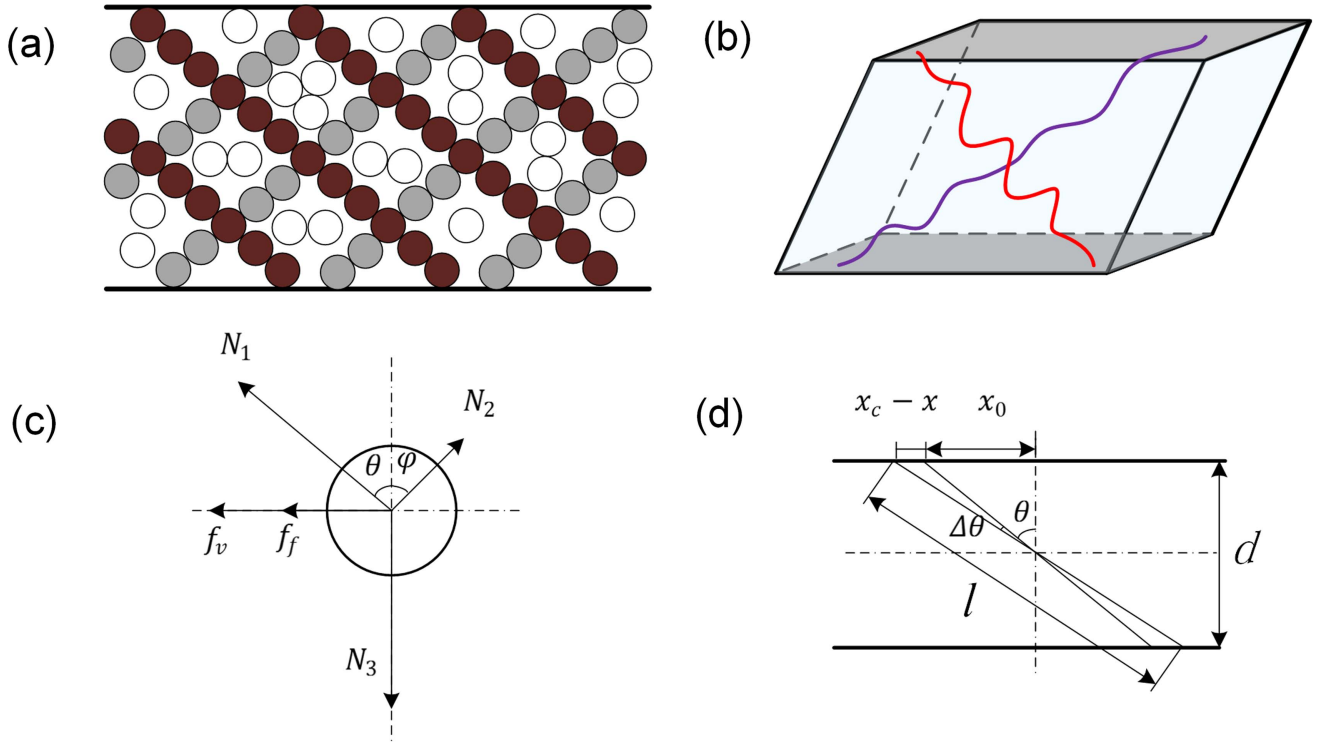
Figure 3. (a) Schematic diagram of network of force chains. Dark: main chains; gray: assistant chains; white: other force-bearing particles. (b) The molecular chain model under shear for the polymer material. (c) The schematic diagram of the force of the particle at the top of the chain. (d) A tiny rotation angle of the force-chain structure.

driven by frictional and elastic forces. This will contributes to a tiny rotation angle $\Delta\theta$ of force-chain structure. From figure 3(d), some geometric relations can be obtained:

$$x_c - x = \frac{l}{2}\frac{\Delta\theta}{\cos\theta}, \tag{6}$$

$$l = \sqrt{4(x_c - x + x_0)^2 + d^2}, \tag{7}$$

$$\cos\theta = \frac{d}{\sqrt{4(x_c - x + x_0)^2 + d^2}}, \tag{8}$$

$$\sin\theta = \frac{x_c - x + x_0}{\sqrt{4(x_c - x + x_0)^2 + d^2}}, \tag{9}$$

where d is the gap between the top and bottom plates. x_0 is half the length of the force-chain structure in the horizontal direction when shear is stopped. Suppose φ is a constant value. Ignore $(x_c - x)^2$ and higher terms when conducting Taylor expansion. The elastic force in the horizontal direction and frictional force in equation (2) can be simplified as:

$$-N_1\sin\theta + N_2\sin\varphi - \mu N_3 = p + q(x_c - x), \tag{10}$$

where p and q are constant values. Combining equations (1) and (2), it can be concluded that

$$m(\ddot{x}_c - \ddot{x}) = p + q(x_c - x) - 6\pi\eta a(\dot{x}_c - \dot{x}). \tag{11}$$

The solution of equation (11) can be written as

$$x_c - x = C_1 e^{\lambda_1 t} + C_2 e^{\lambda_2 t} + C_3. \tag{12}$$

The shear force in the relaxation phase is numerically equal to the frictional force. So the shear stress can be obtained as

$$\tau = \mu N_3/S = D_1 e^{\lambda_1 t} + D_2 e^{\lambda_2 t} + D_3, \tag{13}$$

where C_1, C_2, C_3, D_1, D_2, and D_3 are the coefficients to be determined. λ_1 and λ_2 are the solutions of the characteristic equation. S is the area of plate. From a kinematic point of view, stress relaxation is the result of particle chain rotation and solvent viscosity dissipation.

Based on the force-chain structure, a six-element viscoelastic model (figure 4(a)) is proposed. Here, E_1, E_2 and η_1, η_2 are defined as the stiffness and viscosity parameter of the main chain and assistant chain, respectively. E_3 is defined as the stiffness of other force-bearing particles. Considering the slippage in the boundary and inside of STF, η_3 is defined as the slippage term. The constitutive equation of the six-element viscoelastic model can be expressed as:

$$\sigma + p_1\dot{\sigma} + p_2\ddot{\sigma} = q_0\varepsilon + q_1\dot{\varepsilon} + q_2\ddot{\varepsilon} + q_3\dddot{\varepsilon}, \tag{14}$$

where $\quad p_1 = \frac{\eta_1 E_2 + \eta_2 E_1}{E_1 E_2}, \quad p_2 = \frac{\eta_1\eta_2}{E_1 E_2}, \quad q_0 = E_3,$

$q_1 = \frac{\eta_1 E_2(E_1 + E_3) + \eta_2 E_1(E_2 + E_3) + \eta_3 E_1 E_2}{E_1 E_2},$

$q_2 = \frac{\eta_1\eta_2(E_1 + E_2 + E_3) + \eta_1\eta_3 E_2 + \eta_2\eta_3 E_1}{E_1 E_2}, q_3 = \frac{\eta_1\eta_2\eta_3}{E_1 E_2}.$

It can be concluded that the relaxation modulus can be expressed as:

$$Y(t) = E_1 e^{-\frac{E_1 t}{\eta_1}} + E_2 e^{-\frac{E_2 t}{\eta_2}} + E_3 + \eta_3\delta(t). \tag{15}$$

As shown in figure 4(b), when $t \leqslant t_s$, the strain increases linearly to ε_s, which corresponding to the shear section in the experiment. As $t \geqslant t_s$, the strain maintains a constant value which corresponding to the relaxation section. The stress in these processes can be obtained by the Boltzmann
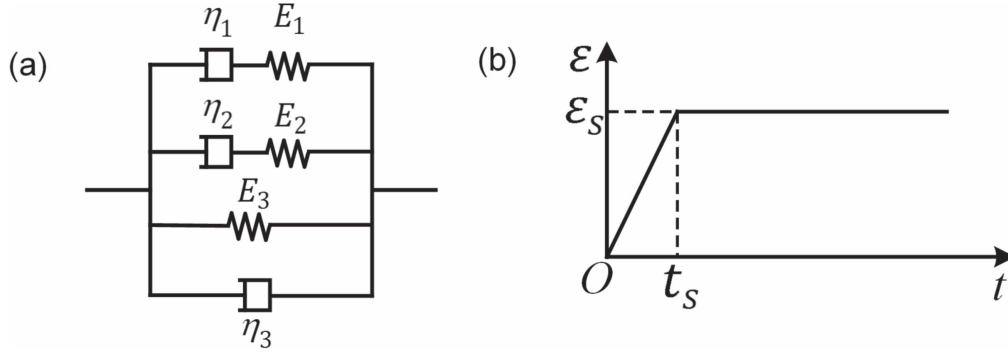
4

Figure 4. (a) Schematic diagram of a six-element viscoelastic model. (b) The change of strain during the test.
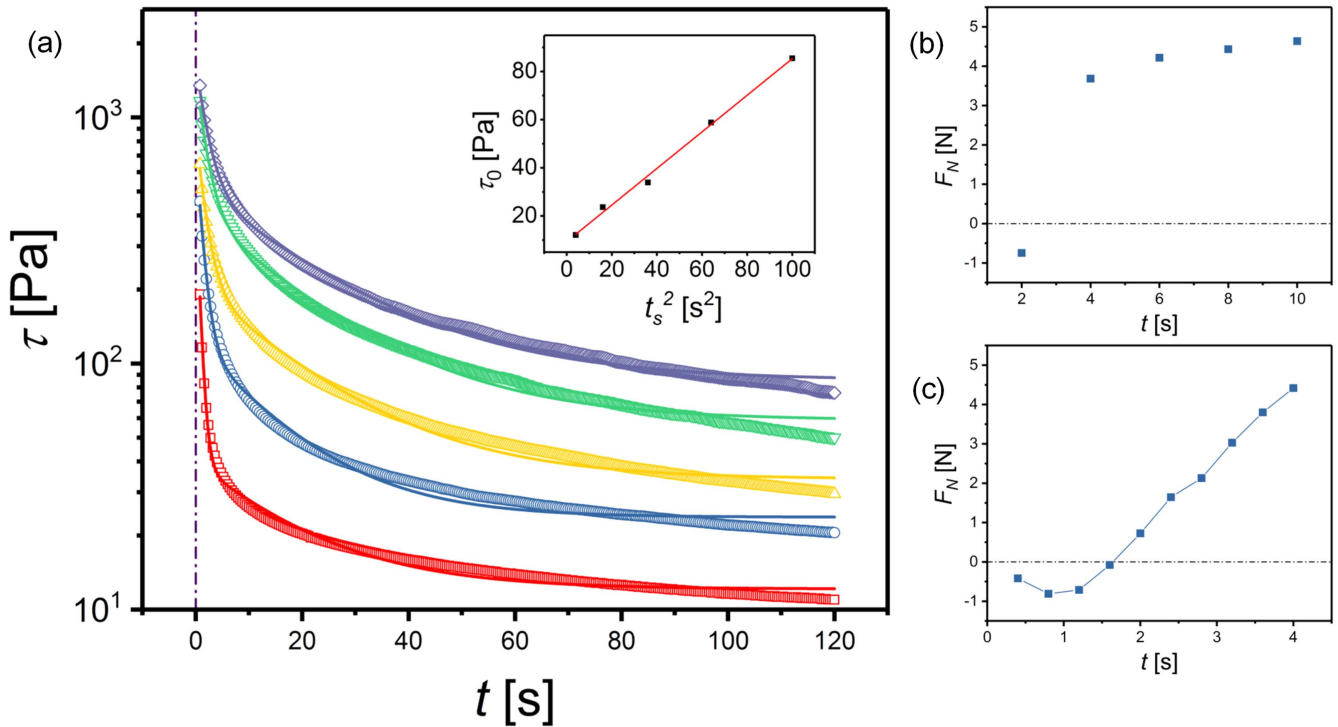

Figure 5. (a) Comparison of experimental values to fitting results. Shear time for experimental data: $t_s = 2$ s (red squares), 4 s (blue circles), 6 s (yellow upper triangles), 8 s (green inverted triangles), 10 s (purple diamonds). The corresponding curves for fitting results have the same colors. Inset, the final stress τ_0 is proportional to t_s^2. (b) The normal force of STF with $\phi = 0.57$ at the end of different pre-shear times corresponding to figure 5(a). (c) The change process of normal force during a pre-shear schedule. ($\phi = 0.59$, $\dot{\gamma} = 10$ s^{-1}).

Table 1. Fitting parameters of the stress relaxation curves in figure 5(a).

t_s	E_1	η_1	E_2	η_2	E_3	t_1	t_2
2 s	0.16	2.9	0.52	0.37	0.076	18.0	0.72
4 s	0.27	4.0	0.24	0.29	0.074	15.1	1.20
6 s	0.31	6.2	0.14	0.24	0.071	19.8	1.67
8 s	0.46	9.3	0.09	0.17	0.093	20.5	1.82
10 s	0.43	9.7	0.06	0.11	0.106	22.6	2.06

superposition principle:

$$\sigma(t) = \varepsilon_0 Y(t) + \int_{0^+}^{t} Y(t - \zeta) \frac{d\varepsilon(\zeta)}{d\zeta} d\zeta. \quad (16)$$

When $t > t_s$, the relaxation stress can be expressed as:

$$\sigma(t) = \frac{\varepsilon_s}{t_s}[\eta_1(e^{\frac{E_1 t_s}{\eta_1}} - 1)e^{-\frac{E_1 t}{\eta_1}} + \eta_2(e^{\frac{E_2 t_s}{\eta_2}} - 1)e^{-\frac{E_2 t}{\eta_2}} + E_3 t_s],$$

$$(17)$$

where $t_1 = \frac{\eta_1}{E_1}$ and $t_2 = \frac{\eta_2}{E_2}$ are defined as the two relaxation times. Remarkably, $\sigma(t)$ is not continuous at $t = t_s$. It will have a sudden decrease of $\frac{\varepsilon_s}{t_s}\eta_3$. This is consistent with the experimental results. As t comes close to infinity, $\sigma(t)$ approaches a constant τ_0. It can be concluded that the final stress $\tau_0 = \varepsilon_0 E_3$. Equations (13) and (17) are the same form for expression. Besides, equation (17) depicts the double exponential expression is due to the differences between the relaxation time of the main and assistant chains.
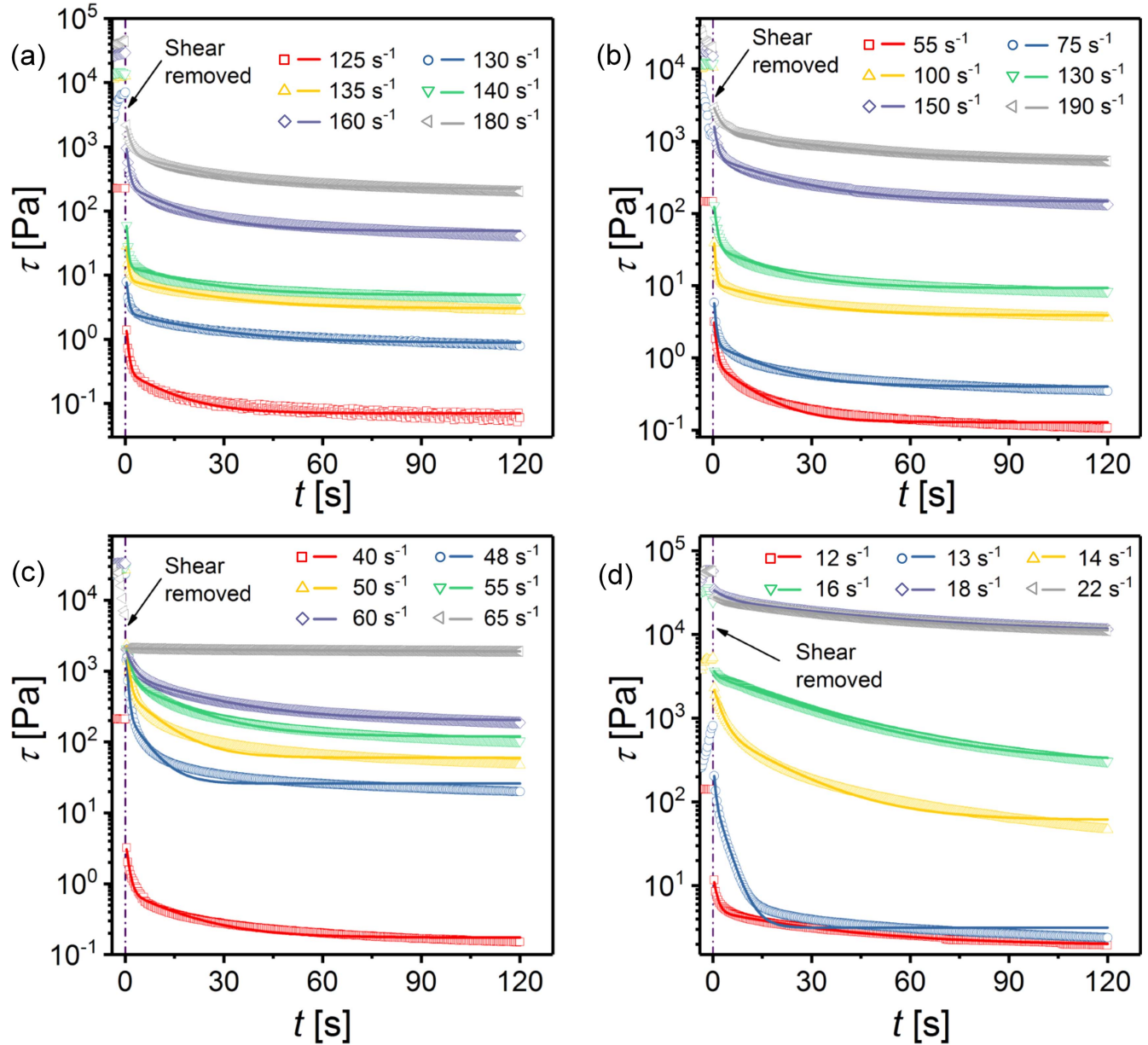
Figure 6. Stress relaxation results of STFs with $\phi = 0.56$ (a), 0.57 (b), 0.58 (c) and 0.59 (d) after shearing at different shear rates. Hollow symbols: experimental results. Solid lines: fitting results according to the viscoelastic model.

3.4. Stress relaxation under varies shear time

Equation (17) depicts that the shear time has a significant effect on the stress relaxation of STF. In order to verify this inference, the STF was first sheared at $\dot{\gamma} = 80\,\mathrm{s}^{-1}$ for 2, 4, 6, 8 and 10 s, then the shear rate was set to 0. Ignoring the initial slip [39] of the relaxation, the results of stress are shown in figure 5(a). The decay rate of τ decreases with the increase of time. The longer the shear time t_s, the greater the τ of the STF during relaxation. Figure 5(a) also shows the result of a double exponential function fitting. The fitting function is as expressed in equation (17). The fitting results are in good agreement with the experimental results. The results of the fitting parameters are given in table 1. η_3 is introduced to explain the sudden drop in shear stress at $t = 0$, which has no effect on the subsequent relaxation phase, so it will not be

discussed furthermore. As t_s increases from 2 to 10 s, E_1 increases and E_2 decreases, which indicates that the force in the direction of compression dominates the network. Both of the STF relaxation times increase and the STF tends to be more elastic. As t_s increased, the particle clusters can form larger agglomerates and may even be in direct contact. As t is large enough, the τ at the end of measurement can be considered equal to τ_0. The inset reveals that $\tau_0 \propto t_s{}^2$. While τ is formally proportional to t_s in equation (17). This depicts that E_3 increases with t_s. The microstructure analysis inferred that D_3 is affected by the elastic force between particles. So the contact force increases with the increase of t_s.

Corresponding to figures 5(a), (b) depicts the results of normal force F_N at the end of different pre-shear times. As the shear time t_s increases from 2 to 10 s, F_N changes from -0.75 to 4.64 N, implying a transition from CST to DST. This is
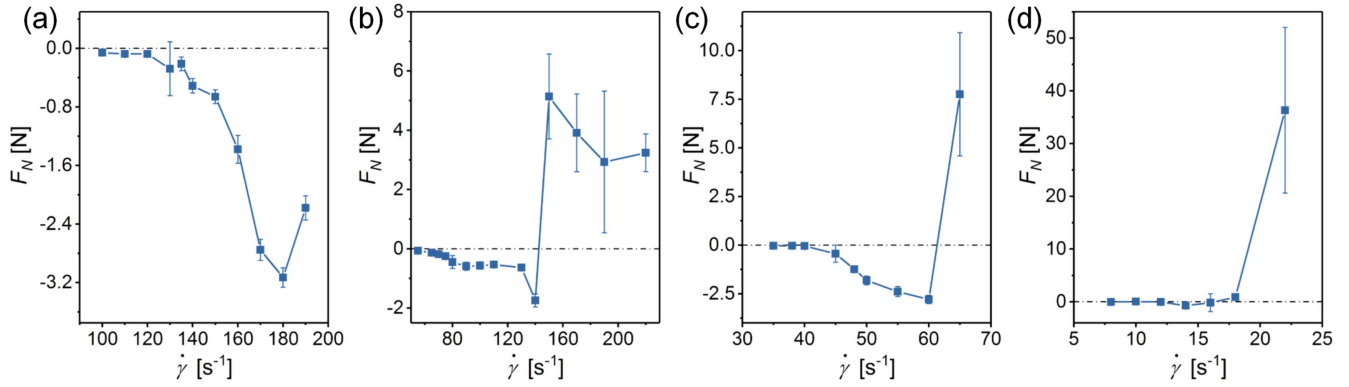
Figure 7. Normal force results of STFs with $\phi = 0.56$ (a), 0.57 (b), 0.58 (c) and 0.59 (d) at different pre-shear rates.

Table 2. Physical parameters of the viscoelastic model in figure 6.

ϕ	$\dot{\gamma}$	E_1	η_1	E_2	η_2	E_3
0.56	125	0.0003	0.005	0.0003	0.0004	0.0001
	130	0.0025	0.079	0.0018	0.0034	0.0016
	135	0.0075	0.247	0.0058	0.0104	0.0052
	140	0.012	0.304	0.0063	0.0075	0.0084
	160	0.21	0.416	0.1856	0.2762	0.0712
	180	0.61	16.19	0.5744	1.2444	0.2911
0.57	55	0.0027	0.028	0.0003	0.0002	0.0006
	75	0.0033	0.049	0.0002	0.0001	0.0013
	100	0.015	0.293	0.0002	0.0001	0.0097
	130	0.042	0.664	0.0092	0.0073	0.0178
	150	0.68	13.53	0.14	0.13	0.244
	190	1.13	37.05	0.69	1.32	0.69
0.58	40	0.003	5.1	0.001	0.001	0.001
	48	0.84	4.625	0.046	0.024	0.134
	50	1.8	16.66	0.34	0.25	0.3
	55	2.44	38	1.38	2.02	0.54
	60	2.5	56.02	1.82	3.73	0.83
	65	2.1	409	0.19	3.23	6.62
0.59	12	0.058	1.97	0.019	0.021	0.04
	13	1.11	3.68	0.015	0.008	0.06
	14	10.9	192.3	11.5	26.64	1.07
	16	42.6	1175	0.98	1.08	4.69
	18	213	10 182	66.8	276	145.4
	22	166	7622	15.2	37.3	115.3

consistent with the results of the particle chain model and the viscoelastic model. The change process of normal force versus shear time in a pre-shear schedule is shown in figure 5(c). Similar to figure 5(b), the transition of F_N from negative to positive of is also observed. An analysis of F_N shows that as t_s increases, F_N changes from negative to positive, consistent with the change of the stiffness of particle chain, which reveals the STF changes from CST to DST.

3.5. Relaxation behavior of STF with different volume fraction

Besides t_s, the concentration of STF can also affect the CST-DST transition [40]. The ST effect of the suspensions is strengthened with the ϕ increases (figure 1(b)). Figure 6 depicts the stress relaxation curves of STFs with different volume fractions after shearing at different shear rates. The result of a double exponential function fitting is also given in figure 6. Table 2 presents the fitting parameters according to equation (17). When $\dot{\gamma} < \dot{\gamma}_c$, with the increase of ϕ, the gap between particles decreases and τ_0 increases from 0.06 to 1.9 Pa. When $\dot{\gamma} \geqslant \dot{\gamma}_c$, the STFs show a shear thickening effect. τ is several orders of magnitude larger than in shear thinning. The six-element viscoelastic model successfully explains the slippage that occurs when the shear is stopped. As t is long enough, τ finally decays to τ_0. Compared with shear thinning, τ_0 at ST is much larger. With the increase of $\dot{\gamma}$, τ increases gradually. When $\phi = 0.56$, F_N at different shear rates are all negative (figure 7(a)), showing CST effect.
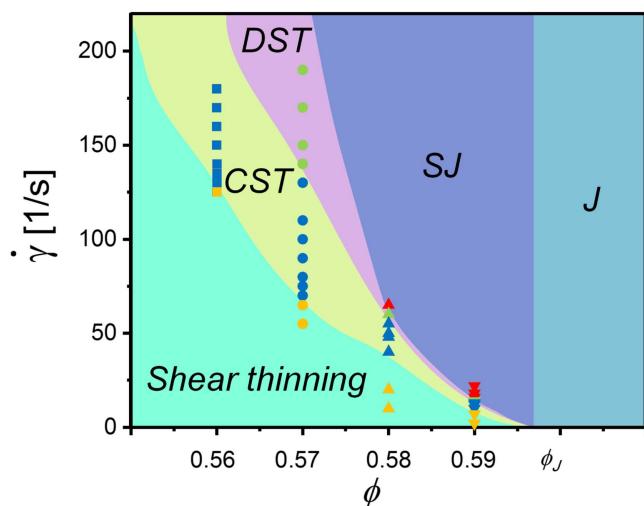
Figure 8. Phase diagram showing the different states of the suspension: shear thinning (orange plots), CST (blue plots), DST (green plots) and SJ (red plots).

When $\phi > 0.56$, F_N exhibits a negative to positive transition with the increasing $\dot{\gamma}$, which corresponding to the transition from CST to DST (figures 7(b)–(d)). It is consistent with the results of viscoelastic model. Although τ_0 continues to increase in the process, the stress relaxation curve does not have a clear line of demarcation. However, the viscoelastic model demonstrates that E_1 is much larger than E_2, implying the force in the direction of main chain dominates the network. When $\dot{\gamma}$ is large enough, the STFs with $\phi = 0.58$ and 0.59 can reach a fully jammed, a solid-like state. For example, τ decreases from 28.3 to 11.1 kPa after 120 s ($\phi = 0.59$, $\dot{\gamma} = 22\ s^{-1}$). The decay of τ is not obvious in figure 6(d) and it could maintain a high value. The physical parameters in the viscoelastic model are orders of magnitude higher than the lower shear rate. Here, the STF exhibits a solid property.

3.6. Phase diagram

Based on the above analysis, a schematic phase diagram [18, 22, 31, 41, 42] in the ϕ–$\dot{\gamma}$ plane is proposed (figure 8). When $\dot{\gamma} < \dot{\gamma}_c$, the STF exhibits shear thinning. Particles in the dispersion medium are in layered distribution. So τ is relatively small under shear and it can quickly decay to an extremely small value as shear is stopped. The STF changes from shear thinning to CST as $\dot{\gamma} > \dot{\gamma}_c$. The strong hydrodynamic coupling between particles leads to the formation of hydroclusters. With the increase of $\dot{\gamma}$ and ϕ, F_N changes from negative to positive (figure 7). The STF transfers from CST to DST as the consequence of the transition from hydrodynamically lubricated to boundary-lubricated contacts. In this process, τ_0 increases with increasing of the $\dot{\gamma}$. When $\dot{\gamma}$ is further increased, SJ occurs. The particles in the suspension are assembled to a dense force-chain network during SJ, and the movement of the particles is limited after removing the shear. The STF shows the solid character. The attenuation of τ is slow and eventually maintains at a very high τ_0. When ϕ is relatively low, DST and SJ are hardly observed. With the increase of ϕ, the shear thinning, CST and DST regions

shrink, SJ dominates the shear thickening area. When $\phi > \phi_J$, the STF is fully jammed without shear.

4. Conclusion

In conclusion, STFs exhibit different stress relaxation behaviors due to their different internal particle structures. The relaxation stress initially drops suddenly due to slip, and then its decay rate decreases gradually and finally remains constant. The microstructure analysis and six-element viscoelastic model successfully explain the stress relaxation curve of STF. An increase of t_s can result in a transition from CST to DST. The relationship between final stress and shear time is $\tau_0 \propto t_s^2$. With the increase of ϕ, the shear thinning, CST and DST regions shrink, SJ dominates the ϕ–$\dot{\gamma}$ plane.

ORCID iDs

Xinglong Gong ⓘ https://orcid.org/0000-0001-6997-9526

References

[1] Barnes H A 1989 Shear-thickening (Dilatancy) in suspensions of nonaggregating solid particles dispersed in Newtonian liquids *J. Rheol.* **33** 329–66
[2] Laun H M, Bung R and Schmidt F 1991 Rheology of extremely shear thickening polymer dispersionsa) (passively viscosity switching fluids) *J. Rheol.* **35** 999–1034
[3] Brown E and Jaeger H M 2014 Shear thickening in concentrated suspensions: phenomenology, mechanisms and relations to jamming *Rep. Prog. Phys.* **77** 046602
[4] Tan Z H, Ge J H, Zhang H, Zhai P C and Li W H 2017 Dynamic response of shear thickening fluid reinforced with SiC nanowires under high strain rates *Appl. Phys. Lett.* **111** 031902
[5] Denn M M, Morris J F and Bonn D 2018 Shear thickening in concentrated suspensions of smooth spheres in Newtonian suspending fluids *Soft Matter* **14** 170–84
[6] Brown E, Forman N A, Orellana C S, Zhang H, Maynor B W, Betts D E, DeSimone J M and Jaeger H M 2010 Generality of shear thickening in dense suspensions *Nat. Mater.* **9** 220–4
[7] Fall A, Bertrand F, Ovarlez G and Bonn D 2012 Shear thickening of cornstarch suspensions *J. Rheol.* **56** 575–91
[8] Jiang W, Peng G, Ma Y, Chen H, Hu J, Jia C and Zhang T 2017 Measuring the mechanical responses of a jammed

discontinuous shear-thickening fluid *Appl. Phys. Lett.* **111** 201906

[9] Wagner N J and Brady J F 2009 Shear thickening in colloidal dispersions *Phys. Today* **62** 27–32

[10] Heussinger C 2013 Shear thickening in granular suspensions: interparticle friction and dynamically correlated clusters *Phys. Rev.* E **88** 050201

[11] Mari R, Seto R, Morris J F and Denn M M 2015 Discontinuous shear thickening in Brownian suspensions by dynamic simulation *Proc. Natl Acad. Sci. USA* **112** 15326–30

[12] Ness C, Xing Z and Eiser E 2017 Oscillatory rheology of dense, athermal suspensions of nearly hard spheres below the jamming point *Soft Matter* **13** 3664–74

[13] Pan Z, de Cagny H, Habibi M and Bonn D 2017 Normal stresses in shear thickening granular suspensions *Soft Matter* **13** 3734–40

[14] Mari R, Seto R, Morris J F and Denn M M 2015 Nonmonotonic flow curves of shear thickening suspensions *Phys. Rev.* E **91** 052302

[15] Pan Z, de Cagny H, Weber B and Bonn D 2015 S-shaped flow curves of shear thickening suspensions: direct observation of frictional rheology *Phys. Rev.* E **92** 032202

[16] Singh A, Mari R, Denn M M and Morris J F 2018 A constitutive model for simple shear of dense frictional suspensions *J. Rheol.* **62** 457–68

[17] Bertrand E, Bibette J and Schmitt V 2002 From shear thickening to shear-induced jamming *Phys. Rev.* E **66** 060401

[18] Brown E and Jaeger H M 2009 Dynamic jamming point for shear thickening suspensions *Phys. Rev. Lett.* **103** 086001

[19] Wyart M and Cates M E 2014 Discontinuous shear thickening without inertia in dense non-Brownian suspensions *Phys. Rev. Lett.* **112** 098302

[20] Boyer F, Guazzelli E and Pouliquen O 2011 Unifying suspension and granular rheology *Phys. Rev. Lett.* **107** 188301

[21] Chu B J and Salem D R 2017 Impact-induced solidlike behavior and elasticity in concentrated colloidal suspensions *Phys. Rev.* E **96** 042601

[22] Peters I R, Majumdar S and Jaeger H M 2016 Direct observation of dynamic shear jamming in dense suspensions *Nature* **532** 214–7

[23] Majumdar S, Peters I R, Han E and Jaeger H M 2017 Dynamic shear jamming in dense granular suspensions under extension *Phys. Rev.* E **95** 012603

[24] Decker M J, Halbach C J, Nam C H, Wagner N J and Wetzel E D 2007 Stab resistance of shear thickening fluid (STF)-treated fabrics *Compos. Sci. Technol.* **67** 565–78

[25] Wei M H, Hu G, Jin L, Lin K and Zou D J 2016 Forced vibration of a shear thickening fluid sandwich beam *Smart Mater. Struct.* **25** 055041

[26] Tian T and Nakano M 2017 Design and testing of a rotational brake with shear thickening fluids *Smart Mater. Struct.* **26** 035038

[27] Gurgen S, Kushan M C and Li W H 2017 Shear thickening fluids in protective applications: a review *Prog. Polym. Sci.* **75** 48–72

[28] Wee M S M, Matia-Merino L and Goh K K T 2015 Time-and shear history-dependence of the rheological properties of a water-soluble extract from the fronds of the black tree fern, Cyathea medullaris *J. Rheol.* **59** 365–76

[29] Chen Q, Xuan S H, Jiang W Q, Cao S S and Gong X L 2016 Shear time dependent viscosity of polystyrene-ethylacrylate based shear thickening fluid *Smart Mater. Struct.* **25** 045005

[30] Zhang X Z, Li W H and Gong X L 2010 Thixotropy of MR shear-thickening fluids *Smart Mater. Struct.* **19** 125012

[31] Jiang W, Xuan S and Gong X 2015 The role of shear in the transition from continuous shear thickening to discontinuous shear thickening *Appl. Phys. Lett.* **106** 151902

[32] D'Haene P, Mewis J and Fuller G G 1993 Scattering dichroism measurements of flow-induced structure of a shear thickening suspension *J. Colloid Interface Sci.* **156** 350–8

[33] Thomas H Y 2014 Mechanisms of shear thickening in transient guar network *J. Rheol.* **58** 1789–807

[34] Maharjan R and Brown E 2017 Giant deviation of a relaxation time from generalized Newtonian theory in discontinuous shear thickening suspensions *Phys. Rev. Fluids* **2** 123301

[35] Fall A, Lemaitre A, Bertrand F, Bonn D and Ovarlez G 2010 Shear thickening and migration in granular suspensions *Phys. Rev. Lett.* **105** 268303

[36] Cates M E, Wittmer J P, Bouchaud J-P and Claudin P 1998 Jamming, force chains, and fragile matter *Phys. Rev. Lett.* **81** 1841

[37] Janmey P A, McCormick M E, Rammensee S, Leight J L, Georges P C and MacKintosh F C 2007 Negative normal stress in semiflexible biopolymer gels *Nat. Mater.* **6** 48–51

[38] de Cagny H C, Vos B E, Vahabi M, Kurniawan N A, Doi M, Koenderink G H, MacKintosh F C and Bonn D 2016 Porosity governs normal stresses in polymer gels *Phys. Rev. Lett.* **117** 217802

[39] Paredes J, Shahidzadeh N and Bonn D 2015 Wall slip and fluidity in emulsion flow *Phys. Rev.* E **92** 042313

[40] Fernandez N, Mani R, Rinaldi D, Kadau D, Mosquet M, Lombois-Burger H, Cayer-Barrioz J, Herrmann H J, Spencer N D and Isa L 2013 Microscopic mechanism for shear thickening of non-Brownian suspensions *Phys. Rev. Lett.* **111** 108301

[41] Seto R, Mari R, Morris J F and Denn M M 2013 Discontinuous shear thickening of frictional hard-sphere suspensions *Phys. Rev. Lett.* **111** 218301

[42] Fall A, Bertrand F, Hautemayou D, Meziere C, Moucheront P, Lemaitre A and Ovarlez G 2015 Macroscopic discontinuous shear thickening versus local shear jamming in cornstarch *Phys. Rev. Lett.* **114** 098301